rheumatoid arthritis in patients in whom the disease has left the midcarpal and radioscaphoid joints relatively unaffected. Radioscapholunate arthrodesis has been found to be useful for patients in whom the entire radiocarpal joint has been destroyed or dislocated but the midcarpal joint is preserved[2,13]. However, some researchers have reported a marked decrease in the range of motion after radioscapholunate arthrodesis[4]. The wrist kinematics after a partial arthrodesis are incompletely understood.

Recently, researchers have been able to measure the three-dimensional kinematics of human joints in vivo with use of a markerless bone-registration technique, which provides three-dimensional views of bones and allows for the evaluation of their precise range and direction of motion by determining the relative positions of the bones in different volume images[3,14-20]. The purpose of the present study was to evaluate the kinematics of the radiocarpal and midcarpal joints of rheumatoid wrists with use of three-dimensional computed tomography before and after radiolunate and radioscapholunate arthrodesis.

Materials and Methods

Subjects

We acquired in vivo kinematic data by means of three-dimensional computed tomography in order to investigate the pathological condition of forty-two wrists in thirty-seven patients with rheumatoid arthritis who had continuous wrist pain, instability, and/or extensor tendon rupture. We assessed the suitability of the midcarpal joint for partial arthrodesis by means of three-dimensional computed tomographic images with use of a bone surface model made with the wrist in a neutral position.

In eighteen of the forty-two wrists, the midcarpal joint was found to be well preserved. Eight of these eighteen wrists were in patients who elected not to have surgery or dropped out of the study. The remaining ten wrists were selected for partial arthrodesis; all had severe radiolunate damage, but all had a relatively well-preserved and congruent midcarpal joint. All patients were female, and the average age was fifty-eight years (range, twenty-three to seventy-one years). The average duration of rheumatoid arthritis was eleven years (range, five to seventeen years), and the average interval between surgery and postoperative image acquisition was nineteen months (range, five to forty-two months).

A radiolunate arthrodesis was used in six wrists; all had a severely damaged radiolunate joint but a normal radioscaphoid articulation. A radioscapholunate arthrodesis was chosen for four wrists in which destruction and subluxation or dislocation of the radioscaphoid joint were detected on direct intraoperative observation. All subjects consented to participate in the present study.

Surgical Technique

All of the procedures were performed by two specialists in hand surgery (H.M. and T.M.), who are the senior authors of the present study. The wrist joint was approached through a dorsal midline skin incision. The dorsal compartments were separated and elevated radially from the radius. In addition, we performed tendon transfer in three wrists, synovectomy in all ten wrists, hemiresection of the ulnar head in seven wrists, and a Darrach procedure in three wrists. The capsule of the radiocarpal and distal radioulnar joints was opened, and synovectomy, hemiresection of the ulnar head, and/or a Darrach procedure was performed as appropriate. The articular surfaces of the scaphoid, lunate, and radius were exposed, and the damaged articular cartilage and cortical bone were removed. For bone graft, we used cancellous bone harvested from the iliac crest in five of the ten wrists and the excised ulnar head in all ten wrists. For fixation, three or four Kirschner wires were used in six wrists and two Kirschner wires with a staple were used in four wrists. For radiolunate arthrodesis, the lunate was fixed in the neutral position with use of enough bone graft to restore height and to keep the distal surfaces of the scaphoid and lunate precisely aligned to produce smooth midcarpal motion with good congruity of the distal surfaces of the scaphoid and lunate. For radioscapholunate arthrodesis, the scaphoid and lunate were each positioned with a temporary Kirschner wire, which was used as a joystick. The scaphoid and the lunate were carefully aligned to the neutral position by fitting each to the proximal articular surface of the capitate. The average flexion of the lunate and scaphoid with respect to the longitudinal axis of the radius measured 51° ± 7° and 5° ± 4°, respectively, consistent with the natural posture as previously reported[21]. The decision to perform a radiolunate or radioscapholunate arthrodesis was made after direct observation of the cartilage status and the congruity of the radioscaphoid joint.

Postoperative immobilization involved the use of a long arm cast for approximately three weeks, followed by a removable splint for two weeks. The patients were able to perform active motion of the wrist and forearm four weeks after the operation. Complete osseous union was achieved in all patients within three months.

Image Acquisition

The technique that we used for in vivo three-dimensional kinematic evaluation has been described in detail previously[3,15-20]. We performed three-dimensional computed tomography on the wrists preoperatively and postoperatively with use of a clinical helical-type scanner with an image slice thickness of 0.625 mm (LightSpeed XTra; GE Healthcare, Waukesha, Wisconsin). We made images with the wrist in three different positions: neutral (in which the third metacarpal and the forearm axis were aligned), maximum wrist flexion, and maximum wrist extension. Data were saved in a standard format (Digital Imaging and Communications in Medicine) that is used commonly for transferring and storing medical images.

Segmentation and Registration

Regions of individual bones were segmented semi-automatically with use of a software program for image analysis (Virtual

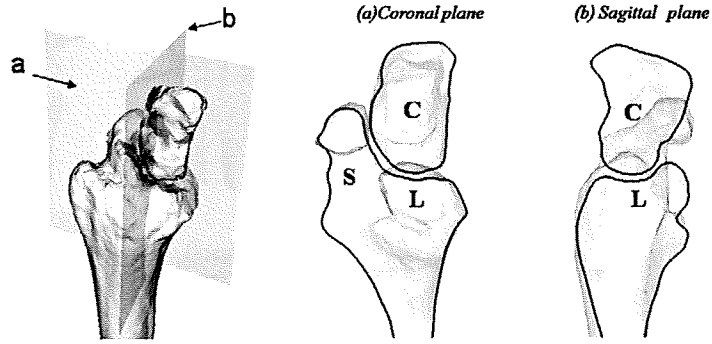

Fig. 1

Illustrations depicting the method used to evaluate midcarpal joint congruity after radiolunate or radioscapholunate arthrodesis. We qualitatively evaluated joint congruity by means of three-dimensional investigation of the bone surface models from any direction and on any cutting plane with use of specially developed software. S = scaphoid, L = lunate, and C = capitate.

Place-M; AZE, Tokyo, Japan). The software generated three-dimensional surface bone models with use of the marching cubes technique[22]. The kinematic variables were calculated by registering the segmented bones[14] from one position to another with use of the software. The accuracy of volume-based registration has been discussed previously[15].

Three-Dimensional Evaluation of Joint Congruity

The three-dimensional bone models created from computed tomography slice data could be viewed and qualitatively evaluated from any direction and on any cutting plane with use of originally developed software (Orthopedics Viewer; Osaka University, Osaka, Japan)[20]. We qualitatively evaluated joint congruity by means of three-dimensional investigation of the bone surface models with use of this software preoperatively and postoperatively (Fig. 1).

Three-Dimensional Quantification of Range of Motion

The radius and all carpal bones except the pisiform were registered, and the relative motion of each bone was calculated. In general, the displacement of the moving body from one position to another can always be represented as a rotation around and translation along a unique axis, which is called a screw axis[23]. We defined this screw axis as an axis of rotation. The three-dimensional range of motion was calculated as the angle of rotation around the axis of rotation[18].

Global wrist motion during wrist flexion-extension before the radiolunate or radioscapholunate arthrodesis, which was represented by capitate motion relative to the radius, was compared with postoperative global wrist motion, represented by capitate motion relative to the fixed lunate.

Midcarpal motion during wrist flexion-extension before the arthrodesis, which was represented by capitate motion

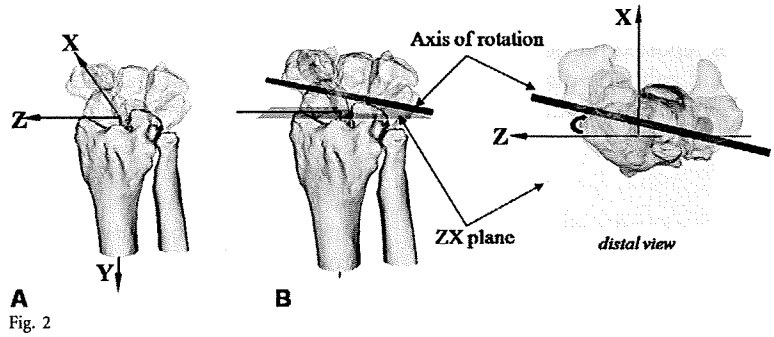

Fig. 2

Illustrations depicting the three-dimensional evaluation of the direction of motion in a wrist following radiolunate arthrodesis. *A:* Orthogonal reference system established for the radius. The Y axis was defined as the longitudinal axis of the radius, the Z axis was defined as the line running through the radial styloid process on the plane perpendicular to the Y axis, and the X axis was defined as the line perpendicular to the YZ plane. *B:* We defined the angle as a "radially and palmarly-directed opening angle" (curved arrow), which was the angle of the axis of rotation relative to the axis of wrist flexion and extension (the Z axis).

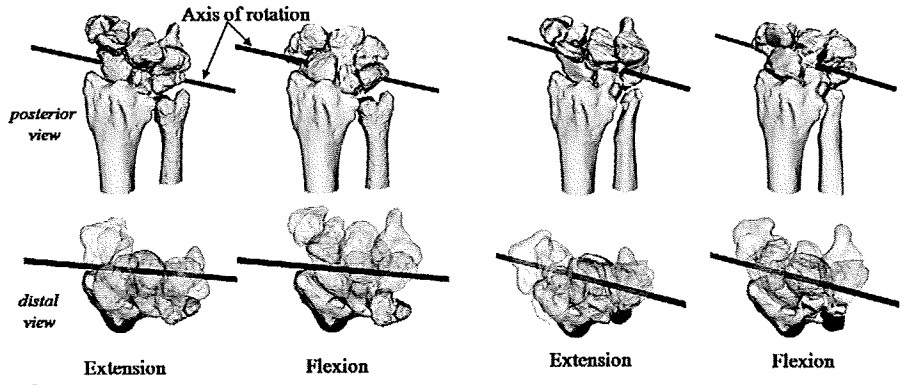

Fig. 3

Posterior and distal views of the right wrist and the axes of rotation during wrist flexion-extension motion before and after radiolunate arthrodesis. *A:* Global wrist motion before the radiolunate arthrodesis. *B:* Global wrist motion after the radiolunate arthrodesis. The postoperative direction of global wrist motion was more oblique from radiodorsal to ulnopalmar along the so-called dart-throwing motion plane as compared with the preoperative direction of global wrist motion.

relative to the scaphoid, lunate, and triquetrum, was compared with postoperative values.

We also evaluated radiocarpal and scapholunate motion preoperatively and postoperatively.

Three-Dimensional Evaluation of Direction of Motion

To quantify the three-dimensional direction of motion, we defined a grid for the radius, which was the orthogonal reference system described by Belsole et al. (Fig. 2, *A*)[24]. A consistent orthogonal reference system was established in the radius in the neutral position, as previously reported[3,25].

After determination of each axis of rotation, the angle of the axis of rotation relative to the axis of wrist flexion and extension (the Z axis of the orthogonal reference system) was calculated as viewed in the axial plane of the radius, defined as the ZX plane. We defined this angle as the radially and palmarly-directed opening angle, as reported previously (Fig. 2, *B*)[19,20]. We evaluated the radially and palmarly-directed opening angle with regard to global wrist motion and midcarpal motion.

Statistical Analysis

All data were expressed as the mean and the standard deviation. Quantitative data on the wrists before and after the operation were compared with use of standard statistical formulas based on the Mann-Whitney U test. Differences were deemed to be significant at $p < 0.05$.

Source of Funding

This research was financially supported by the Nakatani Foundation of Electronic Measuring Technology Advancement, which did not play a role in the investigation. The financial support was used for the supplies, including two computers used for analysis.

Results

Radiolunate Arthrodesis

Global Wrist Motion

The average global range of wrist motion during wrist flexion-extension was 59° ± 4° before radiolunate arthrodesis and 48° ± 21° after radiolunate arthrodesis. The postoperative value was 81% of the preoperative value, but the difference was not significant ($p = 0.34$).

The preoperative direction of global wrist motion was close to the sagittal plane, whereas the postoperative direction of global wrist motion was more oblique from radiodorsal to ulnopalmar along the so-called dart-throwing motion plane (Fig. 3). The radially and palmarly-directed opening angle was 5° ± 13° preoperatively, compared with 25° ± 10° postoperatively; this difference was significant ($p = 0.01$) (Table I).

Midcarpal Motion

The residual postoperative midcarpal motion and joint congruities between the scaphoid, lunate, and capitate were well preserved in all cases. The three-dimensional animation showed that all of the joints in the wrist were moving smoothly and congruently and that scapholunate motion appeared to contribute to global wrist motion after the radiolunate arthrodesis (see Appendix). The average preoperative ranges of capitate motion relative to the scaphoid, lunate, and triquetrum during wrist flexion-extension were 21° ± 9°, 44° ± 8°, and 36° ± 5°, respectively. After radiolunate arthrodesis, the average capitate motions relative to the scaphoid, lunate, and triquetrum were 19° ± 12°, 48° ± 21°, and 31° ± 16°, respectively. The postoperative capitate motion relative to the lunate was 109% of the preoperative value. The postoperative capitate motions relative to the scaphoid and triquetrum were slightly less than the preoperative values (90% and 87%, respectively). However, there was no significant difference in any

TABLE I Kinematic Data in Wrist Flexion-Extension Motion Before and After Radiolunate and Radioscapholunate Arthrodesis*

	Radiolunate Arthrodesis		Radioscapholunate Arthrodesis	
	Before	After	Before	After
Range of motion around axis of rotation *(deg)*				
Capitate to radius	59 ± 4	48 ± 21	83 ± 24	47 ± 14
Capitate to scaphoid	21 ± 9	19 ± 12	18 ± 7	47 ± 14
Capitate to lunate	44 ± 8	48 ± 21	53 ± 21	47 ± 14
Capitate to triquetrum	36 ± 5	31 ± 16	37 ± 14	28 ± 13
Scaphoid to lunate	30 ± 10	30 ± 15	37 ± 15	0 ± 0
Scaphoid to radius	44 ± 11	30 ± 15	66 ± 21	0 ± 0
Lunate to radius	17 ± 9	0 ± 0	31 ± 15	0 ± 0
Radially and palmarly-directed opening angle *(deg)*				
Capitate to radius	5 ± 13	25 ± 10	−2 ± 5	19 ± 11
Capitate to scaphoid	43 ± 25	41 ± 21	3 ± 15	19 ± 11
Capitate to lunate	8 ± 13	25 ± 10	2 ± 6	19 ± 11
Capitate to triquetrum	7 ± 15	24 ± 13	2 ± 3	22 ± 11
Scaphoid to lunate	5 ± 14	16 ± 8	4 ± 8	—
Scaphoid to radius	4 ± 11	16 ± 8	−2 ± 7	—
Lunate to radius	4 ± 35	—	−13 ± 6	—

*The values are given as the mean and the standard deviation.

range of motion in the midcarpal joint before as compared with after radiolunate arthrodesis ($p = 1.00$ for capitate motion relative to the lunate, $p = 0.75$ for capitate motion relative to the scaphoid, and $p = 0.75$ for capitate motion relative to the triquetrum).

The preoperative direction of capitate motion relative to the scaphoid during wrist flexion-extension was oblique from radiodorsal to ulnopalmar and the radially and palmarly-directed opening angle was 43° ± 25°, whereas the preoperative directions of capitate motion relative to the lunate and triquetrum were closer to the sagittal plane than to that of the scaphoid and the radially and palmarly-directed opening angles were 8° ± 13° and 7° ± 15°, respectively. After radiolunate arthrodesis, the direction of capitate motion relative to the scaphoid was oblique from radiodorsal to ulnopalmar, the radially and palmarly-directed opening angle was 41° ± 21°, and the directions of capitate motion relative to the lunate and triquetrum were 25° ± 10° and 24° ± 13°, respectively. The postoperative direction of capitate motion relative to the lunate was significantly more oblique than the preoperative value ($p = 0.03$). The directions of capitate motion relative to the scaphoid and triquetrum did not differ significantly before as compared with after radiolunate arthrodesis ($p = 0.63$ and 0.10, respectively) (Table I).

Radiocarpal Motion

The preoperative range of lunate motion relative to the radius was 17° ± 9°. The preoperative range of scaphoid motion relative to the radius during wrist flexion-extension was 44° ± 11°, whereas the postoperative value was 30° ± 15°. The range of scaphoid motion relative to the radius did not differ significantly before as compared with after radiolunate arthrodesis ($p = 0.11$) (Table I).

Scapholunate Motion

The preoperative range of scaphoid motion relative to the lunate during wrist flexion-extension was 30° ± 10°, whereas the postoperative value was 30° ± 15° (Table I). The difference was not significant.

Radioscapholunate Arthrodesis

Global Wrist Motion

The average preoperative and postoperative ranges of global wrist motion were 83° ± 24° and 47° ± 14°, respectively. The postoperative value was 57% of the preoperative value.

The preoperative direction of global wrist motion was close to the sagittal plane, whereas the postoperative direction of global wrist motion was more oblique from radiodorsal to ulnopalmar along the dart-throwing motion plane as compared with the preoperative direction of global wrist motion (Fig. 4). The radially and palmarly-directed opening angle was −2° ± 5° before surgery and 19° ± 11° after surgery; this difference was significant ($p = 0.02$) (Table I).

Midcarpal Motion

The residual postoperative midcarpal motion and joint congruities between the scaphoid, lunate, and capitate were well preserved in all cases (Fig. 1) (see Appendix). The average preoperative capitate motions relative to the scaphoid,

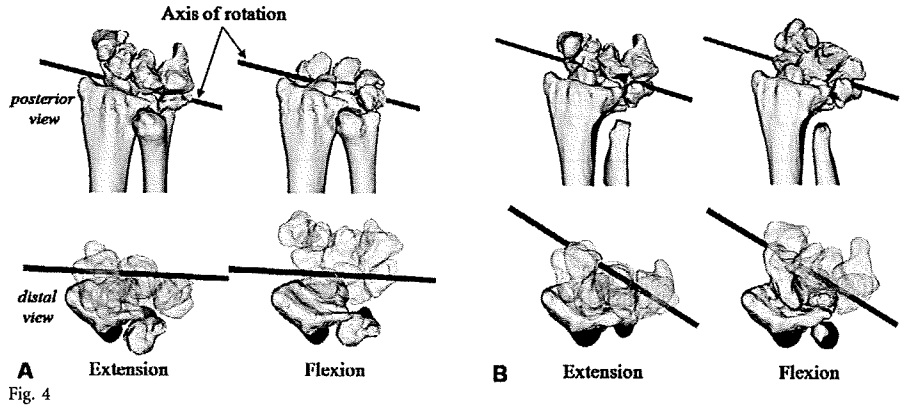

Fig. 4

Posterior and distal views of the right wrist and the axes of rotation during the wrist flexion-extension motion before and after radioscapholunate arthrodesis. *A:* Global wrist motion before radioscapholunate arthrodesis. *B:* Global wrist motion after radioscapholunate arthrodesis. The postoperative direction of global wrist motion was more oblique from radiodorsal to ulnopalmar along the so-called dart-throwing motion plane as compared with the preoperative direction of global wrist motion.

lunate, and triquetrum during wrist flexion-extension were 18° ± 7°, 53° ± 21°, and 37° ± 14°, respectively. After radioscapholunate arthrodesis, the average capitate motion relative to the lunate (with the scaphoid) and triquetrum measured 47° ± 14° and 28° ± 13°, respectively. The postoperative capitate motions relative to the lunate and triquetrum were slightly less than the preoperative motion (88% and 76% of the preoperative values, respectively). However, there was no significant difference in midcarpal motion before radioscapholunate arthrodesis as compared with after radioscapholunate arthrodesis.

The preoperative direction of capitate motion relative to the scaphoid, lunate, and triquetrum during wrist flexion-extension was almost along the sagittal plane, and the radially and palmarly-directed opening angles were 3° ± 15°, 2° ± 6°, and 2° ± 3°, respectively. After radioscapholunate arthrodesis, the direction of capitate motion relative to the lunate (with the scaphoid) and triquetrum was oblique from radiodorsal to ulnopalmar, and the radially and palmarly-directed opening angles were 19° ± 11° and 22° ± 11°, respectively. The postoperative direction of capitate motion relative to the lunate and triquetrum became significantly more oblique than the preoperative value, from radiodorsal to ulnopalmar ($p = 0.02$ and 0.02, respectively) (Table I).

Radiocarpal Motion

Before radioscapholunate arthrodesis, the radiocarpal joint was incongruent between the scaphoid, lunate, and radius during wrist flexion-extension in all cases. The preoperative ranges of scaphoid and lunate motion relative to the radius were 66° ± 21° and 31° ± 15°, respectively (Table I).

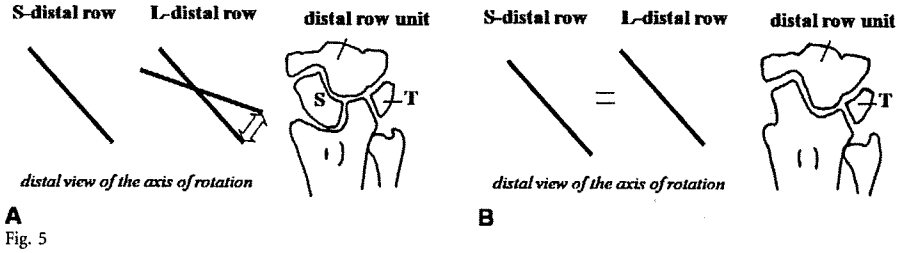

Fig. 5

Distal view of the right wrist and axes of rotation after radiolunate and radioscapholunate arthrodesis. *A:* Distal view of the axes of rotation after radiolunate arthrodesis. The direction of capitate motion relative to the scaphoid during flexion-extension was essentially uniaxial in the dart-throwing motion plane, whereas the direction of capitate motion relative to the lunate has more variability, varying from the sagittal plane to the dart-throwing motion plane. *B:* Distal view of the axes of rotation after radioscapholunate arthrodesis. The residual motion plane of the capitate after radioscapholunate arthrodesis is essentially limited to the dart-throwing motion plane. S = scaphoid, L = lunate, and T = triquetrum.

Discussion

In the present study, the preoperative midcarpal motions were well preserved after both radiolunate and radioscapholunate arthrodesis, and the ranges of capitate motion relative to the lunate were well preserved. The residual postoperative range of global wrist motion was 48° after radiolunate arthrodesis and 47° after radioscapholunate arthrodesis. The motion after radiolunate arthrodesis was 81% of the preoperative value, which was higher than the value of 68% (with the range of motion changing from 57° preoperatively to 39° postoperatively) that had been previously reported[4]. The postoperative range of global wrist motion after radioscapholunate arthrodesis was better than the range of 26° as reported in a previous study[4]. However, the postoperative range of global wrist motion (47°) after radioscapholunate arthrodesis in the present study was only 57% of the preoperative value (83°), which was greater than the preoperative value for wrists treated with radiolunate arthrodesis (59°). We speculate that the greater preoperative global range of motion in the radioscapholunate arthrodesis group was due to the difference in the type of rheumatoid disease. The wrists that were treated with radioscapholunate arthrodesis were of the unstable type[3], with ligamentous laxity, whereas the wrists that received radiolunate arthrodesis were of the stable type[3]. We think that, in unstable wrists, the radiocarpal joint was lax and usually was dislocated and that this may have provided relatively more motion than in stable wrists.

The postoperative direction of wrist motion in the present study was oblique from radiodorsal to ulnopalmar. A recent three-dimensional study revealed that capitate motion relative to the scaphoid was essentially uniaxial and that the motion plane was oblique with respect to the pure flexion-extension plane (the so-called dart-throwing motion plane), whereas the direction of capitate motion relative to the lunate had more flexibility and could range between the pure flexion-extension plane and the dart-throwing motion plane (Fig. 5, *A*)[20]. If the scaphoid is fixed to the lunate, the direction of capitate motion relative to the lunate is dominated by the direction of capitate motion relative to the scaphoid. Therefore, the residual motion plane of the capitate after radioscapholunate arthrodesis is almost limited to the dart-throwing motion plane (Fig. 5, *B*). In addition, if the lunate were fixed in an extended position relative to the scaphoid, even if their joint surfaces were to fit, the scapholunocapitate joint would be locked and smooth midcarpal motion would not be obtained. In the present study, we found a difference between radiolunate and radioscapholunate arthrodesis in terms of the postoperative radially and palmarly-directed opening angle. It has been reported that some carpal supination deformity exists in rheumatoid wrists, especially unstable-type rheumatoid wrists[3,26]. We assume that more carpal supination might remain in wrists treated with radioscapholunate arthrodesis as compared with wrists treated with radiolunate arthrodesis.

The present study had some limitations. We used three-dimensional computed tomography to evaluate joint congruity to ensure that a suitable preoperative condition was set up. However, it is not feasible for all practitioners to obtain a preoperative three-dimensional evaluation of joint congruity. We would suggest that it is important for practitioners to choose carefully the type of surgery based on the preoperative investigation and the direct intraoperative observation focusing on the cartilage preservation and the congruity of the midcarpal and radiocarpal joints. The second limitation is that the present study included only ten wrists—a sample of convenience—and such a small series does not have enough power for the detection of significant differences. We were unable to compare the outcomes of radiolunate and radioscapholunate arthrodesis in terms of patient background information such as the history of disease. The third limitation was that we examined only static three-dimensional views of the carpal bones in a limited number of wrist positions. Static measurements do not reveal functional effects that might occur during actual wrist motion. Garcia-Elias et al. reported that radioscapholunate arthrodesis and distal scaphoid excision provided significantly better results than did radioscapholunate arthrodesis alone in terms of residual pain and the decrease in radial deviation and flexion of the wrist[27]. Adding distal scaphoid excision may lead to kinematics different from those discussed here.

However, in the present study, we found that, after radiolunate and radioscapholunate arthrodesis, midcarpal motion in the dart-throwing motion plane was better preserved than was previously thought. Previous in vivo three-dimensional studies of normal wrist motion have shown that the midcarpal joint essentially moves in the plane of the dart-throwing motion, which is thought to be used frequently in the performance of many activities of daily living[20,28,29]. This may support the use of radiolunate or radioscapholunate arthrodesis as an alternative to total wrist arthrodesis in patients with rheumatoid arthritis.

Appendix

(eA) Videos demonstrating midcarpal motion and joint incongruities after a radiolunate and a radioscapholunate arthrodesis are available with the electronic versions of this article, on our web site at jbjs.org (go to the article citation and click on "Supplementary Material"). ■

NOTE: The authors thank Akira Goto, MD, PhD, Kunihiro Oka, MD, PhD, and Ryoji Nakao, computer programmer, Department of Orthopaedic Surgery, Osaka University, for assistance during parts of the experimental procedure.

Sayuri Arimitsu, MD
Tsuyoshi Murase, MD, PhD
Jun Hashimoto, MD, PhD
Hideki Yoshikawa, MD, PhD
Kazuomi Sugamoto, MD, PhD
Hisao Moritomo, MD, PhD
Department of Orthopaedic Surgery, Osaka University,
2-2 Yamadaoka, Suita-shi,
Osaka 565-0871, Japan.
E-mail address for H. Moritomo: moritomo@ort.med.osaka-u.ac.jp

References

1. Honkanen PB, Mäkelä S, Konttinen YT, Lehto MU. Radiocarpal arthrodesis in the treatment of the rheumatoid wrist. A prospective midterm follow-up. J Hand Surg Eur Vol. 2007;32:368-76.

2. Murray PM. Radioscapholunate arthrodesis. Hand Clin. 2005;21:561-6.

3. Arimitsu S, Sugamoto K, Hashimoto J, Murase T, Yoshikawa H, Moritomo H. Analysis of radiocarpal and midcarpal motion in stable and unstable rheumatoid wrists using 3-dimensional computed tomography. J Hand Surg Am. 2009;33:189-97.

4. Ishikawa H, Murasawa A, Nakazono K. Long-term follow-up study of radiocarpal arthrodesis for the rheumatoid wrist. J Hand Surg Am. 2005;30:658-66.

5. Chamay A, Della Santa D, Vilaseca A. Radiolunate arthrodesis. Factor of stability for the rheumatoid wrist. Ann Chir Main. 1983;2:5-17.

6. Linscheid RL, Dobyns JH. Radiolunate arthrodesis. J Hand Surg Am. 1985;10(6 Pt 1):821-9.

7. Stanley JK, Boot DA. Radio-lunate arthrodesis. J Hand Surg Br. 1989;14:283-7.

8. Ishikawa H, Hanyu T, Saito H, Takahashi H. Limited arthrodesis for the rheumatoid wrist. J Hand Surg Am. 1992;17:1103-9.

9. Della Santa D, Chamay A. Radiological evolution of the rheumatoid wrist after radio-lunate arthrodesis. J Hand Surg Br. 1995;20:146-54.

10. Halikis MN, Colello-Abraham K, Taleisnik J. Radiolunate fusion. The forgotten partial arthrodesis. Clin Orthop Relat Res. 1997;341:30-5.

11. Doets HC, Raven EEJ. A procedure for stabilising and preserving mobility in the arthritic wrist. J Bone Joint Surg Br. 1999;81:1013-6.

12. Borisch N, Haussmann P. Radiolunate arthrodesis in the rheumatoid wrist: a retrospective clinical and radiological longterm follow-up. J Hand Surg Br. 2002;27:61-72.

13. Simmen BR, Huber H. The rheumatoid wrist: a new classification related to the type of the natural course and its consequences for surgical therapy. In: Simmen BR, Hagena F, editors. The wrist in rheumatoid arthritis. Basel: Karger; 1992. p 13-25.

14. Besl PJ, Mackay N. A method for registration of 3-D shapes. IEEE Trans Patt Anal. 1992;14:239-56.

15. Goto A, Moritomo H, Murase T, Oka K, Sugamoto K, Arimura T, Masumoto J, Tamura S, Yoshikawa H, Ochi T. In vivo three-dimensional wrist motion analysis using magnetic resonance imaging and volume-based registration. J Orthop Res. 2005;23:750-6.

16. Oka K, Moritomo H, Murase T, Goto A, Sugamoto K, Yoshikawa H. Patterns of carpal deformity in scaphoid nonunion: a 3-dimensional and quantitative analysis. J Hand Surg Am. 2005;30:1136-44.

17. Oka K, Doi K, Suzuki K, Murase T, Goto A, Yoshikawa H, Sugamoto K, Moritomo H. In vivo three-dimensional motion analysis of the forearm with radioulnar synostosis treated by the Kanaya procedure. J Orthop Res. 2006;24:1028-35.

18. Moritomo H, Goto A, Sato Y, Sugamoto K, Murase T, Yoshikawa H. The triquetrum-hamate joint: an anatomic and in vivo three-dimensional kinematic study. J Hand Surg Am. 2003;28:797-805.

19. Moritomo H, Murase T, Goto A, Oka K, Sugamoto K, Yoshikawa H. Capitate-based kinematics of the midcarpal joint during wrist radioulnar deviation: an in vivo three-dimensional motion analysis. J Hand Surg Am. 2004;29:668-75.

20. Moritomo H, Murase T, Goto A, Oka K, Sugamoto K, Yoshikawa H. In vivo three-dimensional kinematics of the midcarpal joint of the wrist. J Bone Joint Surg Am. 2006;88:611-21.

21. Larsen CF, Mathiesen FK, Lindequist S. Measurements of carpal bone angles on lateral wrist radiographs. J Hand Surg Am. 1991;16:888-93.

22. Lorensen WE, Cline HE. Marching cubes: a high resolution 3D surface construction algorithm. Computer Graphics. 1987;21:163-9.

23. Kinzel GL, Hall AS Jr, Hillberry BM. Measurement of the total motion between two body segments. I. Analytical development. J Biomech. 1972;5:93-105.

24. Belsole RJ, Hilbelink DR, Llewellyn JA, Dale M, Ogden JA. Carpal orientation from computed reference axes. J Hand Surg Am. 1991;16:82-90.

25. Arimitsu S, Murase T, Hashimoto J, Oka K, Sugamoto K, Yoshikawa H, Moritomo H. A three-dimensional quantitative analysis of carpal deformity in rheumatoid wrists. J Bone Joint Surg Br. 2007;89:490-4.

26. Shapiro JS. The wrist in rheumatoid arthritis. Hand Clin. 1996;12:477-98.

27. Garcia-Elias M, Lluch A, Ferreres A, Papini-Zorli I, Rahimtoola ZO. Treatment of radiocarpal degenerative osteoarthritis by radioscapholunate arthrodesis and distal scaphoidectomy. J Hand Surg Am. 2005;30:8-15.

28. Li ZM, Kuxhaus L, Fisk JA, Christophel TH. Coupling between wrist flexion-extension and radial-ulnar deviation. Clin Biomech (Bristol, Avon). 2005;20:177-83.

29. Palmer AK, Werner FW, Murphy D, Glisson R. Functional wrist motion: a biomechanical study. J Hand Surg Am. 1985;10:39-46.

Morphometric Analysis of Acetabular Dysplasia in Cerebral Palsy: Three-dimensional CT Study

Shinichi Gose, MD, Takashi Sakai, MD, PhD,† Toru Shibata, MD, PhD,* Tsuyoshi Murase, MD, PhD,† Hideki Yoshikawa, MD, PhD,† and Kazuomi Sugamoto, MD, PhD‡*

Background: Three-dimensional computed tomography (3D-CT) eliminates the positioning errors and allows the clinician to more accurately assess the radiographic parameters present. To elucidate the 3D geometry of the acetabulum and the extent of hip subluxation/dislocation in patients with cerebral palsy (CP), quantitative morphometric analysis was performed using 3D-CT data.

Methods: We evaluated 150 hips in 75 patients with bilateral spastic CP. The mean age of the patients was 5.4 years (range: 2.7 to 6.9 y). The fitting plane of the ilium was projected onto the coronal plane and then onto the sagittal plane, and then the angle formed with a horizontal line was defined as CTα (the lateral opening angle) and CTβ (the sagittal inclination angle), respectively. The center of the acetabulum and the femoral head were defined, and the distance between these centers was divided by the femoral head diameter, defined as CT migration percentage (CTMP, %).

Results: In 123 (82%) of the 150 hips, the femoral head center was located posteriorly, superiorly, and laterally relative to the acetabular center. Large CTα cases tended to show large CTMP. CTα and CTMP were significantly larger in the cases with Gross Motor Functional Classification System (GMFCS) level IV/V and spastic quadriplegia, than in the cases with GMFCS level II/III and spastic diplegia. CTβ showed significant correlation with the acetabular defect on the lateral 3D reconstructed images.

Conclusions: Three-dimensional acetabular geometry and migration percentage in CP patients can be analyzed quantitatively using 3D-CT regardless of the abnormal spastic posture. The extent of acetabular dysplasia and subluxation is more severe in patients with GMFCS level IV/V and spastic quadriplesia.

Level of Evidence: Level 4.

Key Words: cerebral palsy, acetabular dysplasia, hip subluxation/dislocation, 3D-CT, quantitative evaluation

(*J Pediatr Orthop* 2009;29:896–902)

From the *Department of Orthopaedic Surgery, Morinomiya Hospital, Osaka; Departments of †Orthopaedic Surgery; and ‡Orthopaedic Biomaterial Science, Osaka University Graduate School of Medicine, Suita, Japan.

One of the authors (T.M.) has received funding from the Japanese Science and Technology Agency.

Reprints: Takashi Sakai, MD, PhD, Department of Orthopaedic Surgery, Osaka University Graduate School of Medicine, 2-2, Yamadaoka, Suita 565-0871, Japan. E-mail: tsakai-osk@umin.ac.jp.

Cerebral palsy (CP) is a heterogeneous condition resulting from a static brain lesion that occurs around birth. The brain lesion is permanent and has deleterious effects on subsequent development and aging.[1] CP may be classified according to motor type, topographic distribution, and functional severity.[2] The motor types can be classified as spastic, dystonic, mixed, ataxic, or hypotonic, and the definitions of each type have recently been updated.[2] The most common topographic distributions are spastic hemiplegia, spastic diplegia (SD), and spastic quadriplegia.[2] The limitation of the range of motion and the contracture of the joints can occur in the whole body, and thus patients encounter several difficulties in performing routine daily activities, resulting in the diminishment of quality of life.[3] Hip subluxation or dislocation occurs most commonly in neurologically immature, no ambulation, spastic children, and usually becomes apparent from 5 to 7 years after birth.[1,4] The majority of children with hip subluxation/dislocation showed a spastic motor type of CP.[4] Hip instability including progressive subluxation occurs in approximately 15% of spastic CP patients, whereas hip subluxation occurs in 25% to 50% of patients with spastic quadriplegia.[1,4] Subluxation/dislocation of the hip may lead to hip pain, femoral fracture, decubitus, ulcers, and severe problems performing daily activities such as ambulation, standing, sitting balance, dressing, and perineal hygiene.[1,5,6]

The cause of hip disorder in CP is thought to involve a combination of the following various factors[1,4,7]: muscle imbalance,[8–10] flexion and adduction contracture of the hip joint,[2,3,5,6,11–13] acetabular dysplasia,[14] and femoral growth abnormality.[15,16] The pathomechanics of dislocation in CP are not fully understood.[17] Several studies have reported that while acetabular growth is normal till 30 months after birth, after 30 months, hip subluxation becomes worse in accordance with acetabular dysplasia.[1,6,11,18] According to their speculation, to investigate the extent of acetabular dysplasia and of hip subluxation/dislocation accurately in the infant period is important for the prognostication of hip disorder in CP. Many authors have reported that early surgical intervention in patients with spastic hip disease leads to better long-term outcomes and decreases the risk of treatment failure.[2]

Generally, anteroposterior radiographs of the hip joint are evaluated for the assessment of acetabular

dysplasia and hip subluxation/dislocation.[19] However, it is difficult to maintain the pelvis in neutral position in CP because of the abnormal posture because of hypertonia. In particular, it is difficult to correct the lateral inclination and the rotation of the pelvis, and to evaluate acetabular dysplasia and migration percentage accurately when taking anteroposterior radiographs of the hip joint in CP patients who have the contracture.[20]

In better investigate acetabular geometry and hip subluxation/dislocation in CP patients, 2-dimensional (2D) evaluation using horizontal axial computed tomography (CT) images[21,22] and evaluation using 3D-CT images[7,17,23,24] of the pelvis have been performed. The use of multislice CT, such as 64-channnel CT for the hip joint, enables assessment of acetabular dysplasia and hip subluxation/dislocation three-dimensionally under the same condition regardless of the abnormal spastic posture at different times. Although qualitative evaluation of CP hips has been reported,[7,17,23,24] there are no reports of quantitative 3D evaluation performed by setting the pelvis coordinate system.

We have previously reported 3D quantitative studies of the shoulder,[25] the hand,[26,27] the spine,[28] and the ankle[29,30] using 3D-CT or magnetic resonance imaging. The aim of this study was to quantitatively evaluate the 3D geometry of acetabular dysplasia and subluxation/dislocation of the hip in CP using 3D-CT reconstructed images, and to compare the 3D-CT evaluation with the 2D radiologic evaluation.

METHODS

Between June 2006 and November 2008, 150 hips in 75 bilateral spastic CP patients, including SD in 60 patients and spastic quadriplesia (SQ) in 15 patients, without any surgical treatment, were investigated using 3D-CT at our hospital. There were 52 boys and 23 girls with an average age of 5.4 years (range: 2.7 to 6.9 y). According to the Gross Motor Functional Classification System (GMFCS),[31] there were 17 patients at level II, 34 at level III, 16 at level IV, and 8 at level V. The GMFCS is a valid and reliable tool for the classification of gross motor function and has been described for various bands.[31] Children who have GMFCS level I function have a nearly normal level of gross motor function. Children with level II function walk independently but have limitations in activities such as running or jumping. Those with level III function require assistive devices to walk and use a wheelchair for longer distances. Those with level IV function have the ability to stand for transfers, have minimal walking ability, and depend mainly on a wheelchair for mobility. Children with level V function lack head control; cannot independently sit, stand, or walk; and are dependent for all aspects of care.[2,31] Our institution has verified that all investigations were conducted in conformity with ethical principles of research.

Axial images of the pelvis and femora were obtained with a multislice CT scanner (Brilliance CT 64, Philips, Tokyo, Japan). Both the slice thickness and the pitch were 2 mm from the top of the pelvis to the top of the fibula head. We referred to the age-specific and weight-specific pediatric protocols of the multidetector CT,[32] and limited the dose of irradiation. All CT image data were recorded as DICOM -format data, and reconstructed into 3D pelvis and femur models using Virtual Place-M software (Medical Imaging Laboratory, Tokyo, Japan). The 3D

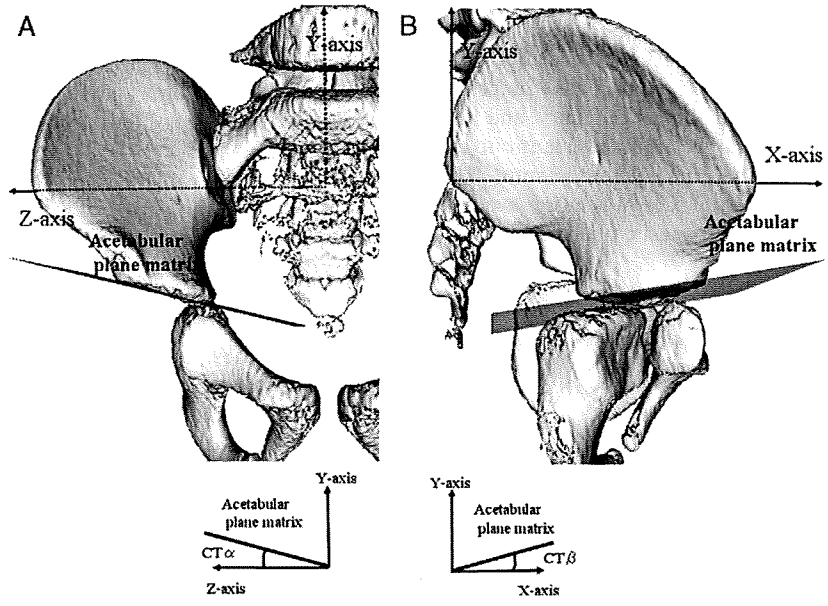

FIGURE 1. The International Society of Biomechanics axis for the pelvis, acetabular plane matrix, computed tomography (CT)α, and CTβ. A, Acetabular plane matrix was projected to the coronal plane (YZ plane) and the angle formed with the Z axis was defined as CTα (the lateral opening angle). B, Acetabular plane matrix was projected to the sagittal plane (XY plane) and the angle formed with the X axis was defined as CTβ (the sagittal inclination angle).

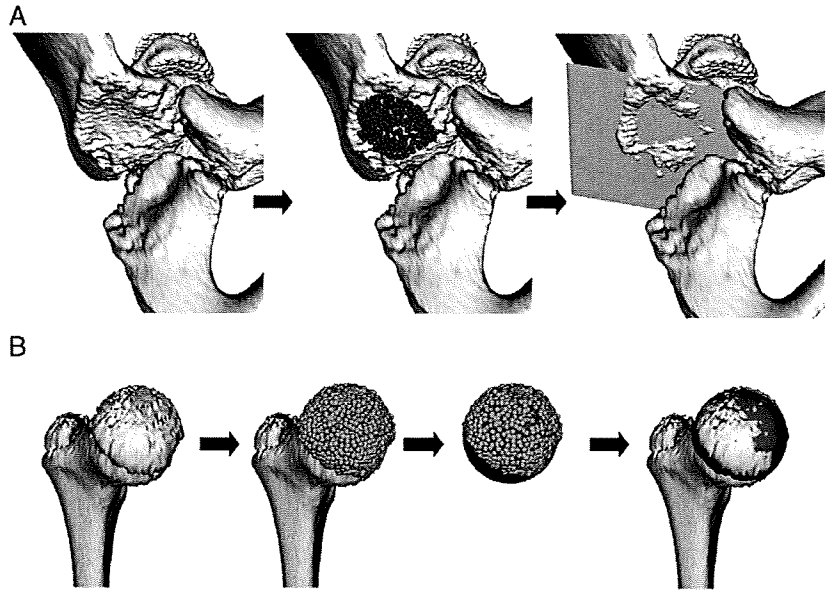

FIGURE 2. Acetabular plane matrix and femoral head sphere. A, On the articular surface of the ilium, about 200 points were plotted and the acetabular plane matrix was created automatically. B, On the femoral head surface, about 400 points were plotted and the femoral head sphere then produced automatically.

models were analyzed using original software on a computer monitor as described below.

The anatomic axis was determined according to the International Society of Biomechanics criteria for the pelvis (Fig. 1).[33] In this system, the origin is coincident with the midpoint of the right posterior superior iliac spine (PSIS) and the left PSIS. The Z axis is the line connecting the 2 PSISs, and pointing to the right

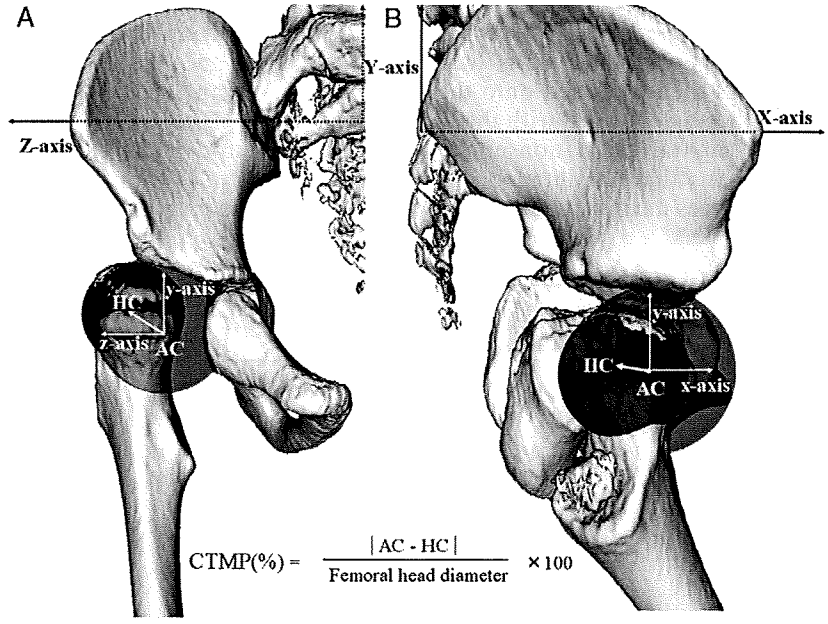

FIGURE 3. Computed tomography migration percentage (CTMP). The distance between the center of the acetabular sphere (acetabular center, AC) and the center of the femoral head sphere (head center, HC) divided by the femoral head diameter was defined as CTMP (%), and the direction of the connecting line between AC and HC were evaluated 3-dimensionally. The direction of the connecting line is divided into 3-dimensional vector, *x*-axis element, *y*-axis element, and *z*-axis element, and each value on *x*, *y*, and *z* axis was divided by the diameter of femoral head as CTMP-*x* (%), CTMP-*y* (%), and CTMP-*z* (%). A, Coronal plane view (YZ plane). B, Sagittal plane view (XY plane).

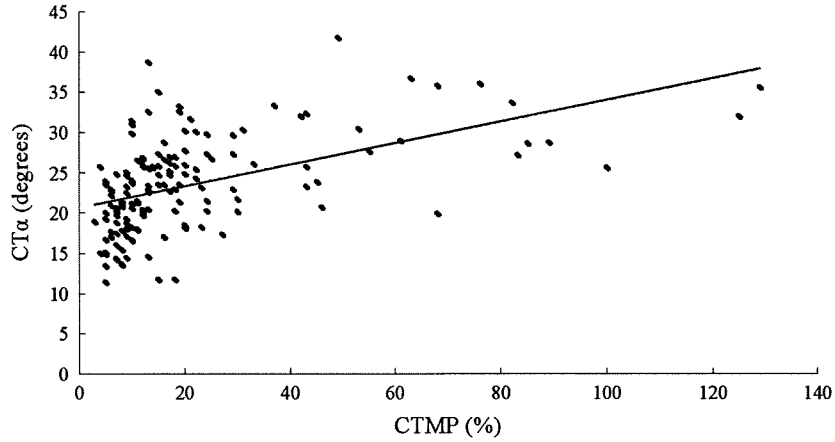

FIGURE 4. Scattergram of CTα and computed tomography migration percentage (CTMP). There was a correlation between CTα and CTMP ($r=0.51$, $P<0.0001$, Spearman rank test).

(Fig. 1A). The X axis is the line connecting the origin and the midpoint of the right anterior superior iliac spine and the left anterior superior iliac spine, and pointing anteriorly (Fig. 1B). The Y axis is the line perpendicular to both X and Z, pointing cranially.

On the articular surface of the ilium, about 200 points were plotted and the acetabular plane matrix, the best-fit plane for the articular surface of the ilium, was created automatically (standard deviation, 0.60) (Fig. 2A). Similarly, about 400 points were plotted on the femoral head surface and the femoral head sphere then produced automatically (standard deviation, 0.59) (Fig. 2B).

The acetabular plane matrix was projected onto the coronal plane (YZ plane) and the angle formed with the Z axis defined as CTα (the lateral opening angle) (Fig. 1A). The acetabular plane matrix was then projected onto the sagittal plane (XY plane) and the angle formed with the X axis was defined as CTβ (the sagittal inclination angle) (Fig. 1B). CTβ > 0 degrees means that the ilium opens posteriorly whereas CTβ < 0 degrees means that the ilium opens anteriorly. The relationship between CTβ and the acetabular defect type on the lateral 3D reconstructed images was also investigated. The location of the acetabular defect was classified as anterior, posterior, or global (mixed) according to Chung et al,[17] using the 3D reconstructed lateral images of the acetabulum.

Next, about 300 points were plotted on the articular surface of the ilium, pubis, and ischium, and then the acetabular sphere (Fig. 3) was created automatically (standard deviation, 0.89). The center of the acetabular sphere (acetabular center, AC) was measured. The center of the femoral head sphere (head center, HC) and the diameter of the femoral head were measured. The distance between AC and HC divided by the femoral head diameter was defined as the CT migration percentage (CTMP, %), and the direction of the connecting line between AC and HC was evaluated 3-dimensionally (Fig. 3). The direction of the connecting line is divided into a 3D vector, x-axis element (anterior and posterior), y-axis element (superior and inferior), and z-axis element (lateral and medial), and each value of the x, y, and z-axis

TABLE 1. Assessment of CTα, CTβ, and CTMP in the Group of GMFCS, CP Type, and Sex

	N (Hips)	CTα (Degrees)	CTβ (Degrees)	CTMP (%)
Total	150	23.5 ± 5.9 (11.4-41.7)	2.4 ± 6.2 (−17.6-18.8)	21.3 ± 22.4 (3-129)
GMFCS				
II/III	102	22.1 ± 4.6 (11.4-35)	2.5 ± 6.4 (−12.1-18.8)	12.8 ± 7.5 (3-43)
IV/V	48	26.4 ± 7.3 (11.7-41.7)	2.1 ± 5.8 (−17.6-13.8)	39.6 ± 31.1 (7-129)
		$P < 0.001$	$P = 0.84$	$P < 0.0001$
CP type				
SD	120	22.6 ± 4.9 (11.4-36.7)	2.7 ± 6.2 (−12.1-18.8)	16.3 ± 14.5 (3-100)
SQ	30	26.9 ± 8.1 (11.7-41.7)	1.0 ± 5.9 (−17.6-13.6)	41.4 ± 34.9 (8-129)
		$P = 0.003$	$P = 0.26$	$P < 0.001$
Sex				
Boy	104	23.5 ± 5.6 (11.7-36.7)	3.6 ± 10.1 (−10.1-18.8)	23.7 ± 24.7 (3-129)
Girl	46	23.5 ± 6.7 (11.4-41.7)	−0.3 ± 5.7 (−17.6-10.3)	16.0 ± 15.5 (4-76)
		$P = 0.87$	$P < 0.001$	$P = 0.025$

Mann-Whitney U test was significant with $P < 0.05$.

CP indicates cerebral palsy; CTMP, computed tomography migration percentage; GMFCS, Gross Motor Functional Classification System; SD, spastic diplegia; SQ, spastic quadriplegia.

TABLE 2. CTβ and Sex

Sex	Total (Hips)	CTβ > 0 Degrees (%)	CTβ < 0 Degrees (%)
Total (hips)	150	96 (64)	54 (36)
Boy (hips)	104	72 (69)	32 (31)
Girl (hips)	46	24 (52)	22 (48)

CTβ > 0 Degrees indicates the ilium opened posteriorly.
CTβ < 0 Degrees indicates the ilium opened anteriorly.

element was divided by the diameter of the femoral head, to produce CTMP-x (%), CTMP-y (%), and CTMP-z (%). Each x, y, and z axis pointed anteriorly, superiorly, and laterally, respectively.

To investigate the factors related to the extent of acetabular dysplasia and hip subluxation/dislocation, the relationship between CTα, CTβ, and CTMP, and the correlation between these values and various other factors including GMFCS level (II/III and IV/V), the type of CP (SD and SQ), age, and sex, were investigated.

To compare 3D-CT evaluation with 2D evaluation of plain radiographs of the hip, the acetabular index (Xpα)[20] and the migration percentage (XpMP)[19,20,34] on anteroposterior radiographs were measured in 102 hips (68% of all patients), and then compared with CTα and CTMP, respectively. XpMP is measured by drawing a horizontal line through the triradiate cartilages of both hips and then drawing a vertical line perpendicular to it at the lateral margin of the acetabulum.[20]

Statistical Analysis

Comparisons between CTα and CTβ, CTMP and CTα, and CTMP and CTβ were performed using Spearman rank test. Comparison between CTα, CTβ, CTMP, and the acetabular defect type was performed using the Kruskal-Wallis test. The Mann-Whitney U test was used to assess CTα, CTβ, and CTMP in the group of GMFCS (II/III and IV/V), CP type (SD and SQ), and sex. We considered P values of 0.05 or less to indicate statistical significance.

RESULTS

Hips with a large CTMP tended to show a large CTα, with a positive correlation found between CTα and CTMP ($r = 0.51$, $P < 0.0001$) (Fig. 4). There was no correlation between CTβ and CTMP ($r = 0.16$, $P = 0.05$), or between CTα and CTβ ($r = 0.11$, $P = 0.17$). The mean CTα, CTβ, and CTMP were shown in Tables 1 and 2.

TABLE 4. Three-dimensional Relative Position of the Femoral Head Center

	Mean ± SD (%)	Range (%)
CTMP-x (anterior-posterior)	−11.4 ± 11.7	−68 to 6
CTMP-y (superior-inferior)	9.3 ± 9.9	−3 to 56
CTMP-z (lateral-medial)	12.6 ± 18.7	−9 to 104

The direction of the connecting line between the acetabular center (the origin) and the femoral head center is divided into a 3-dimensional vector, and each value of the x, y, and z-axis element was divided by the diameter of the femoral head, to produce CTMP-x (%), CTMP-y (%), and CTMP-z (%). Each x, y, and z axis pointed anteriorly, superiorly, and laterally, respectively.
CTMP indicates computed tomography migration percentage.

Qualitative analysis of the location of the acetabular defects and the mean of CTα, CTβ, and CTMP are shown in Table 3. There were significant differences in the location of the acetabular defects concerning CTα, CTβ, and CTMP ($P < 0.0001$).

In 123 (82%) of the 150 hips, the femoral HC was located posteriorly, superiorly, and laterally compared with the AC on the pelvis coordinate system (Table 4).

CTα was significantly larger in the GMFCS level IV/V patients (non-walking children) than in the GMFCS level II/III patients (mostly walking children) ($P < 0.001$) (Table 1), whereas CTMP was also significantly larger in the GMFCS level IV/V ($P < 0.0001$). CTα ($P = 0.003$) and CTMP ($P < 0.001$) were also significantly larger in SQ cases than in SD cases (Table 1). CTβ was significantly larger in boys than in girls ($P < 0.001$) (Tables 1, 2). There was a positive correlation between age and CTMP ($P < 0.001$), between age and CTα ($P = 0.05$), and between age and CTβ ($P = 0.03$).

There was also a correlation between CTα and Xpα ($r = 0.58$, $P < 0.0001$), and a strong correlation between CTMP and XpMP ($r = 0.85$, $P < 0.0001$) (Fig. 5). The mean Xpα was 21.1 ± 6.4 degrees (range: 5.9 to 43.4 degrees), whereas the mean XpMP was 41.2 ± 21.0% (range: 9% to 100%).

DISCUSSION

In this morphometric analysis of acetabular dysplasia and hip subluxation/dislocation in CP using 3D-CT, large CTMP hips tended to show large CTα, namely acetabular dysplasia. CTMP was significantly larger in the GMFCS level IV/V patients than in the GMFCS level II/III patients. CP children with more severe involvement and who are unable to walk have the greatest risk of hip

TABLE 3. CTα, CTβ, and CTMP Compared With the Qualitative Analysis of the Acetabular Defects

Location	N (Hips)	CTα (Degrees)	CTβ (Degrees)	CTMP (%)
Posterior	85	23.9 ± 5.1 (14.4-36.7)	4.5 ± 5.7 (−9.9-18.8)	22.0 ± 19.2 (5-89)
Anterior	53	21.5 ± 6.3 (11.4-41.7)	−1.0 ± 5.6 (−17.6-13.6)	11.7 ± 8.1 (3-49)
Global	12	29.3 ± 5.0 (21.2-36.1)	2.7 ± 4.9 (−6.5-10.8)	59.6 ± 38.9 (8-129)
		$P < 0.0001$	$P < 0.0001$	$P < 0.0001$

Kruskal-Wallis test.
CTMP indicates computed tomography migration percentage.

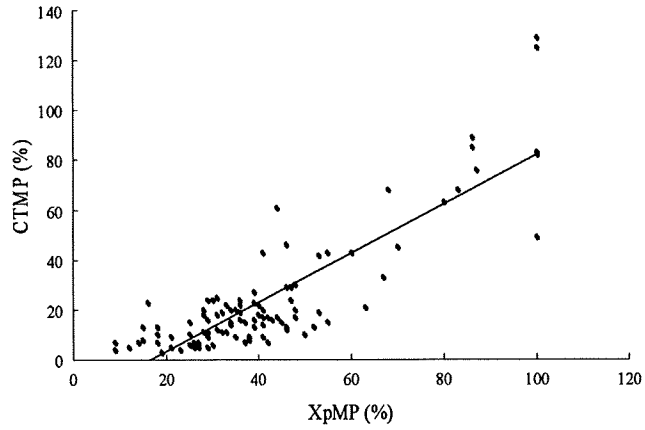

FIGURE 5. Scattergram of XpMP and computed tomography migration percentage (CTMP). There was a strong correlation between XpMP and CTMP (r=0.85, P<0.0001, Spearman rank test).

displacement.[4,6,15,18,35] Significantly higher relative risks of hip displacement have been shown between GMFCS levels II and level V.[2,15,36,37] The same results were found in this study, and the SQ group showed more severe CTα and CTMP than the SD group, most likely because GMFCS level IV/V and SQ-type patients often have severe muscle imbalance and spasticity that leads to disturbance of acetabular bony growth and to migration of the femoral head.

The femoral HC was located posteriorly, superiorly, and laterally compared with the AC on the International Society of Biomechanics pelvis coordinate system in 123 (82%) of the 150 hips examined. The direction of the subluxation/dislocation force in a child with a spastic hip in the spastic position is the posterolateral direction, which may be related to hip flexion and adduction contracture.[8-10,38] Some researchers have speculated that the process of dysplastic hip occurrence is as follows: hip subluxation and dislocation happen gradually in the child with cerebral paralysis during the normal growth process, with muscle imbalance because of spasticity obstructing bone formation, resulting in decreasing normal movement and weight bearing.[1,4,10] As this study was a cross-sectional study, not a longitudinal study, whether hip dysplasia or hip subluxation/dislocation occurs first remains unknown.

Qualitative evaluation revealed that the posterior defect type was most common among the present patients, as seen in the study by Chung.[17] CTβ showed significant correlation with acetabular defect type on the lateral 3D reconstructed images.

There was a strong correlation between CTMP and XpMP (r = 0.85, P < 0.0001). Although XpMP is useful in evaluating the extent of coverage of the femoral head by the acetabulum, CTMP may be more useful in evaluating femoral head migration than XpMP because CTMP shows the distance between the AC and the femoral HC. CTMP is not directly influenced by the extent of acetabulum coverage. Hip subluxation/dislocation may appear as 2 types: femoral head migration without acetabular dysplasia (XpMP and CTMP increase) or severe acetabular dysplasia without femoral head migration (XpMP increase but CTMP does not change). The pattern of XpMP and CTMP may be able to distinguish these 2 factors of hip subluxation/dislocation.

Although Xpα has been reported to be more suitable for prognostication of hip dislocation of the hip compared with femoral shaft angle and XpMP,[14] there is an opposite finding that the correlation is weak between Xpα at 18 to 30 months and the extent of hip subluxation/dislocation at the age of 5 months.[18] In this study, we found a correlation between CTα and Xpα (r = 0.58). In the child with CP, it is difficult to acquire the same pelvic position at different examination times because of flexion contracture of the hip and knee joint.[19,24] However, CTα and CTMP measurement is not influenced by posture when taking 3D-CT images at different times. Using the pelvis coordinate system, quantitative evaluation using 3D-CT reconstructed data seems to provide more accurate information than radiologic evaluation. Although the radiation exposure to the children is a concern, we think that a controlled and limited dose of irradiation is acceptable to investigate the accurate 3D acetabular geometry and migration percentage in CP patients, referred to the age-specific and weight-specific pediatric protocols of the multidetector CT.[32]

There are some limitations of this study. First, the sample size was small and there was no normal control. This limitation was compensated for by useful computer simulation and by ensuring accurate digital measurement of various angles. Second, a morphometric study of the femur, being one of the factors involved in hip subluxation/dislocation in CP,[1,4,15] was not performed. Third, in this 3D-CT morphometric study, the subchondral bone surface of the pelvis was evaluated, but the articular cartilage was not investigated by magnetic resonance imaging. Further study is required with regard to femoral geometry and articular cartilage in CP.

In conclusion, 3D acetabular geometry and the extent of subluxation/dislocation in CP patients can be analyzed quantitatively using 3D-CT regardless of the abnormal spastic posture. We believe that CTα is an appropriate parameter of acetabular dysplasia, while CTMP is a suitable parameter of hip displacement and CTβ a suitable parameter of the acetabular defect on lateral images. CTα and CTMP were significantly larger in GMFCS level IV/V and SQ patients than in the GMFCS level II/III and SD patients. These findings indicate that the extent of acetabular dysplasia and subluxation is more severe in patients with GMFCS level IV/V and SQ.

ACKNOWLEDGMENT

The authors thank Mr Ryoji Nakao, and Dr Kunihiro Oka for technical support in analyzing the 3D-CT data.

REFERENCES

1. Abel MF, Damiano DL. Cerebral Palsy. In: Sponseller PD, ed. *Orthopaedic Knowledge Update: Pediatrics 2.* Rosemont: American Academy Orthopaedic Surgeons; 2002:233–247.
2. Soo B, Howard JJ, Boyd RN, et al. Hip displacement in cerebral palsy. *J Bone Joint Surg Am.* 2006;88:121–129.
3. Hagglund G, Andersson S, Duppe H, et al. Prevention of dislocation of the hip in children with cerebral palsy. The first ten years of a population-based prevention programme. *J Bone Joint Surg Br.* 2005;87:95–101.
4. Gamble JG, Rinsky LA, Bleck EE. Established hip dislocations in children with cerebral palsy. *Clin Orthop Relat Res* 1990;253:90–99.
5. Presedo A, Oh C-W, Dabney KW, et al. Soft-tissue releases to treat spastic hip subluxation in children with cerebral palsy. *J Bone Joint Surg Am.* 2005;87:832–841.
6. Terjesen T. Development of the hip joint in unoperated children with cerebral palsy: a radiographic study of 76 patients. *Acta Orthop.* 2006;77:125–131.
7. Kim HT, Wenger DR. Location of acetabular deficiency and associated hip dislocation in neuromuscular hip dysplasia: three-dimensional computed tomographic analysis. *J Pediatr Orthop.* 1997;17:143–151.
8. Hoffer MN. Management of the hip in cerebral palsy. *J Bone Joint Surg Am.* 1986;68:629–631.
9. Bagg MR, Farber J, Miller F. Long-term follow-up of hip subluxation in cerebral palsy patients. *J Pediatr Orthop.* 1993;13:32–36.
10. Kalen V, Bleck EE. Prevention of spastic paralytic dislocation of the hip. *Dev Med Child Neurol.* 1985;27:17–24.
11. Cornell MS. The hip in cerebral palsy. *Dev Med Child Neurol.* 1995;37:3–18.
12. Schmale GA, Eilert RE, Chang F, et al. High reoperation rates after early treatment of the subluxating hip in children with spastic cerebral palsy. *J Pediatr Orthop.* 2006;26:617–623.
13. Miller F, Dias RC, Dabney KW, et al. Soft-tissue release for spastic hip subluxation in cerebral palsy. *J Pediatr Orthop.* 1997;17: 571–584.
14. Cooke PH, Cole WG, Carey RPL. Dislocation of the hip in cerebral palsy. *J Bone Joint Surg Br.* 1989;71:441–446.
15. Robin J, Graham HK, Selber P, et al. Proximal femoral geometry in cerebral palsy. A population-based cross-sectional study. *J Bone Joint Surg Br.* 2008;90:1372–1379.
16. Davids JR, Marshall AD, Blocker ER, et al. Femoral anteversion in children with cerebral palsy: assessment with two and three-dimensional computed tomography scans. *J Bone Joint Surg Am.* 2003;85:481–488.
17. Chung CY, Park MS, Choi IH, et al. Morphometric analysis of acetabular dysplasia in cerebral palsy. *J Bone Joint Surg Br.* 2006; 88:243–247.
18. Scrutton D, Baird G, Smeeton N, et al. Hip dysplasia in bilateral cerebral palsy: incidence and natural history in children aged 18 months to 5 years. *Dev Med Child Neurol.* 2001;43:586–600.
19. Reimers J. The stability of the hip in children: a radiological study of the results of muscle surgery in cerebral palsy. *Acta Orthop Scand Suppl.* 1980;184:1–100.
20. Parrott J, Boyd RN, Dobson F, et al. Hip displacement in spastic cerebral palsy: repeatability radiologic measurement. *J Pediatr Orthop.* 2002;22:660–667.
21. Gugenheim JJ, Gerson LP, Sadler C, et al. Pathologic morphology of the acetabulum in paralytic and congenital hip instability. *J Pediatr Orthop.* 1982;2:397–400.
22. Buckley SL, Sponseller PD, Magid D. The acetabulum in congenital and neuromuscular hip instability. *J Pediatr Orthop.* 1991;11: 498–501.
23. Abel MF, Wenger DR, Mubarak SJ, et al. Quantitative analysis of the hip dysplasia in cerebral palsy: a study of radiographs and 3-D reformatted images. *J Pediatr Orthop.* 1994;14:283–289.
24. Chung CY, Choi IH, Cho T-J, et al. Morphometric changes in the acetabulum after Dega osteotomy in patients with cerebral palsy. *J Bone Joint Surg Br.* 2008;90:88–91.
25. Sahara W, Sugamoto K, Murai M, et al. 3D kinematic analysis of the acromioclavicular joint during arm abduction using vertically open MRI. *Orthop Res.* 2006;24:1823–1831.
26. Moritomo H, Murase T, Goto A, et al. In vivo three-dimensional kinematics of the midcarpal joint of the wrist. *J Bone Joint Surg Am.* 2006;88:611–621.
27. Goto A, Moritomo H, Murase T, et al. In vivo three-dimensional wrist motion analysis using magnetic resonance imaging and volume-based registration. *J Orthop Res.* 2005;23:750–756.
28. Ishii T, Mukai Y, Hosono N, et al. Kinematics of the cervical spine in lateral bending: in vivo three-dimensional analysis. *Spine.* 2006;31:155–160.
29. Itohara T, Sugamoto K, Shimizu N, et al. Assessment of the three-dimensional relationship of the ossific nuclei and cartilaginous anlagen in congenital clubfoot by 3-D MRI. *J Orthop Res.* 2005; 23:1160–1164.
30. Liu H, Sugamoto K, Itohara T, et al. In vivo three-dimensional skeletal alignment analysis of the hindfoot valgus deformity in patients with rheumatoid arthritis. *J Orthop Res.* 2007;25: 330–339.
31. Palisano R, Rosenbaum P, Walter S, et al. Development and reliability of a system to classify gross motor function in children with cerebral palsy. *Dev Med Child Neurol.* 1997;39:214–223.
32. Hugh TM. Dose reduction for CT pediatric imaging. *Pediatr Radiol.* 2002;32:724–728.
33. Wu G, Siegler S, Allard P, et al. ISB recommendation on definitions of joint coordinate system of various joints for the reporting of human joint motion: Part 1. Ankle, hip, and spine. *J Biomech.* 2002;35:543–548.
34. Miller F, Bagg MR. Age and migration percentage as risk factors for progression in spastic hip disease. *Dev Med Child Neurol.* 1995;37:449–455.
35. Howard CB, Mckibbin B, Williams LA, et al. Factors affecting the incidence of hip dislocation in cerebral palsy. *J Bone Joint Surg Br.* 1985;67:530–532.
36. Morton RE, Scott B, McClelland V, et al. Dislocation of the hips in children with bilateral spastic cerebral palsy, 1985-2000. *Dev Med Child Neurol.* 2006;48:555–558.
37. Graham HK, Boyd R, Carlin JB, et al. Does botulinum toxin A combined with bracing prevent hip displacement in children with cerebral palsy and "hips at risk"? *J Bone Joint Surg Am.* 2008; 90:23–33.
38. Miller F, Sloczykowski M, Cope R, et al. Computer modeling of the pathomechanics of spastic hip dislocation in children. *J Pediatr Orthop.* 1999;19:486–492.

SCIENTIFIC ARTICLE

Radial Overgrowth After Radial Shortening Osteotomies for Skeletally Immature Patients With Kienböck's Disease

Tomoya Matsuhashi, MD, Norimasa Iwasaki, MD, Naomi Oizumi, MD, Hiroyuki Kato, MD, Michio Minami, MD, Akio Minami, MD

Purpose We hypothesized that radial shortening osteotomy (radial shortening) for skeletally immature patients with Kienböck's disease would induce overgrowth of the radius. The purpose of this study was to determine the effect of radial shortening on radial growth in skeletally immature patients with Kienböck's disease and to clarify the relationship between the postoperative growth alterations and the clinical results.

Methods Eight wrists of 8 skeletally immature patients with Kienböck's disease were treated with radial shortening. There were 3 boys and 5 girls, ranging in age from 11 to 18 (mean, 14) years old. All patients presented with open physis and negative ulnar variance. The length of the radial shortening equaled the amount of negative ulnar variance. Clinical assessment was based on the modified Nakamura scoring system. Radiographic assessment, including Lichtman's stages, ulnar variance, carpal height ratio, radial inclination, and volar tilt, was performed before surgery, immediately after surgery, and at follow-up. A difference in ulnar variance of more than 2 mm between these 3 measurements was considered to be overgrowth. Statistical comparisons were performed using paired *t*-tests.

Results At a mean follow-up period of 69 months, the mean clinical score was 19.7 of 21 maximum points, with all wrists rated as excellent. Radiographically, no progression of Lichtman stage was found in any patient. At follow-up, the x-ray and magnetic resonance imaging findings indicated lunate revascularization in all patients. Four of the 8 had overgrowth in the operated radius. On the other hand, other radiographic parameters showed no significant changes at follow-up. The occurrence of postoperative radial overgrowth did not notably affect the clinical scores.

Conclusions The current results suggest the probability of overgrowth of the radius in skeletally immature patients with Kienböck's disease treated with radial shortening. The postoperative radial overgrowth after this osteotomy had no effect on clinical and other radiographic outcomes. *(J Hand Surg 2009;34A:1242–1247. © 2009 Published by Elsevier Inc. on behalf of the American Society for Surgery of the Hand.)*

Type of study/level of evidence Therapeutic IV.

Key words Radial shortening osteotomy, skeletally immature patients, Kienböck's disease, postoperative overgrowth.

From the Department of Orthopaedic Surgery, Hokkaido University Graduate School of Medicine, Sapporo, Japan; Department of Orthopaedic Surgery, Shinsyu University Graduate School of Medicine, Matsumoto, Japan; Hokkaido Orthopaedic Memorial Hospital, Sapporo, Japan.

Received for publication June 24, 2008; accepted in revised form April 20, 2009.

No benefits in any form have been received or will be received related directly or indirectly to the subject of this article.

Corresponding author: Norimasa Iwasaki, MD, Department of Orthopaedic Surgery, Hokkaido University Graduate School of Medicine, Kita 15 Nishi 7, Sapporo, 060-8638, Japan; e-mail: niwasaki@med.hokudai.ac.jp.

0363-5023/09/34A07-0010$36.00/0
doi:10.1016/j.jhsa.2009.04.028

KIENBÖCK'S DISEASE OFTEN affects men between the ages of 20 and 40 who are manual laborers.[1] The pathogenesis of this disease process is still controversial. Consequently, various surgeries, including excision arthroplasty,[2,3] radial wedge and shortening osteotomies,[4–8] limited intercarpal arthrodeses,[9–11] and lunate revascularization procedures[12–14] have been advocated as treatments.

Based on the theory that negative ulnar variance is a potential causative factor in Kienböck's disease,[15,16] radial shortening osteotomy (radial shortening) has been advocated for patients with negative ulnar variance and has been reported to improve clinical results in adults.[4,5,7] However, little is known about the postoperative history of the disease in skeletally immature patients. In a recent study, Iwasaki et al.[6] reported that radial shortening provided satisfactory clinical and radiographic outcomes in teenage patients, even at advanced stages of the disease.

We found few reports concerning the outcome and risk of postoperative overgrowth of the radius after radial shortening for skeletally immature patients in Kienböck's disease.[17]

In this study, we performed radial shortening for skeletally immature patients with Kienböck's disease and evaluated clinical and radiographic results. The hypothesis was that radial shortening for skeletally immature patients with Kienböck's disease would induce alterations in radial growth. The aims of this study were to determine the effect of radial shortening on radial growth in skeletally immature patients with Kienböck's disease and to elucidate relationships between postoperative growth changes and clinical outcomes.

MATERIALS AND METHODS

We retrospectively identified and reviewed all skeletally immature patients with symptomatic Kienböck's disease who were considered for radial shortening from 1990 to 2004. Chart reviews identified 8 patients. Three surgeons carried out radial shortening for the 8 patients with negative ulnar variance. Hospital medical records and preoperative and postoperative radiographs obtained at regular follow-ups were collected in order to evaluate the clinical and radiographic findings. There were 3 boys and 5 girls between 11 and 18 (mean, 14) years old. They presented with open physis. All patients had an occupational or recreational background of repeated minor stress to the wrist. Six patients had a history of acute trauma to the affected wrist. In all patients, occupational or recreational activities were interrupted by severe wrist pain. Preoperative Lichtman's stages[18] were determined according to the radiographic findings (Table 1). In identifying preoperative Lichtman's stages in this study, 2 cases were at stage II, 2 cases were at stage IIIA, and 4 cases were at stage IIIB. All patients had preoperative magnetic resonance imaging (MRI), and 6 of the 8 patients had MRI scans at follow-up.

TABLE 1. Lichtman's Stages

Staging	Radiographic Assessment
Stage I	Normal except for the possibility of a linear or compression fracture
Stage II	Definite changes in the apparent density of the lunate
Stage IIIA	Collapse of the entire lunate at a normal scapholunate angle
Stage IIIB	Collapse of the entire lunate at a scapholunate angle greater than 60°
Stage IV	Generalized degenerative changes in the carpus

Surgical technique

All surgeries on the patients were performed under general anesthesia. An 8-cm longitudinal skin incision was made in the distal part of the anterior aspect of the forearm, parallel and lateral to the tendon of the flexor carpi radialis. The distal part of the radius was exposed between the brachioradialis and the flexor carpi radialis tendon. Radial shortening was carried out by making 2 parallel transverse cuts and removing an appropriate segment of the bone. The length of the removed segment equaled the amount of negative ulnar variance measured on the preoperative radiograph. The osteotomy site was fixed by a 5-hole or 6-hole dynamic compression plate. Using fluoroscopy, we avoided a growth plate injury by plate application. After surgery, a below-elbow splint was applied for 2 weeks. All patients had surgery to remove the plate approximately 1 year after surgery.

Outcome assessment

At follow-up, patients were evaluated clinically and radiographically. Clinical evaluation was based on a modification of the scoring system of Nakamura et al. (Table 2).[19] Three observers examined clinical findings at follow-up. The original scoring system with a 30-point maximum was based on clinical and radiographic results, with 21 points and 9 points, respectively. Although the radiographic assessment was deleted from the original scoring system, we assessed the radiographic findings in other parameters, including ulnar

TABLE 2. Modified Nakamura et al. Scoring System

Clinical Assessment	Points
Pain in the wrist	
None	10
Mild with strenuous activity	7
Mild with light work	4
Grip strength (percentage of unaffected side)	
90%	5
80%	4
70%	3
60%	2
50%	1
Increase in range of flexion and extension	
>20°	6
10° to 19°	5
5° to 9°	3
Overall grade	Total points
Excellent	15–21
Good	9–14
Fair/poor	<8

variance,[15,20,21] carpal height ratio,[3,22] radial inclination,[23] and volar tilt.[23]

Radiographic evaluation was based on the Lichtman stage.[18] The progression of degenerative change through the entire wrist joint and revascularization of the diseased lunate was determined with anteroposterior (AP) and lateral radiographs of the wrist. The radiographic parameters, including ulnar variance,[15,20,21] carpal height ratio,[3,22] radial inclination,[23] and volar tilt,[23] were measured before surgery, immediately after the radial shortening, and at follow-up. The *ulnar variance* is defined as the difference on the AP radiograph between the transverse line at the level of the lunate fossa and the transverse line at the level of the ulnar head, with the shoulder abducted, elbow flexed, and forearm in neutral rotation to quantify variance.[15,20,21] The *carpal height ratio* is defined as the carpal height divided by the length of the third metacarpal on the AP radiograph.[3,22] The *radial inclination* is the angle of the distal radial articular surface to the line perpendicular to the long axis of the radius on the AP radiograph.[23] The volar tilt is the angle created between the articular surface of the distal radius and the line perpendicular to the long axis of the radius on the lateral radiograph.[23] Regarding overgrowth, a difference in length of more than 2 mm was considered a discrepancy.[24] According to the MRI grading system by Nakamura et al,[19] the preoperative and postoperative signal intensities of the lunate were evaluated.

The radiographic measurements were all made by the senior author (N.I.), an experienced hand surgeon. Intra-observer variations in the measurements were assessed by calculating the coefficient variation, which equals the standard deviation divided by the mean value. The observer took 5 measurements of each parameter in the same radiograph. The coefficient of variation of each parameter among the results of 5 sets was calculated. The value was 9% in the ulnar variance, 3% in the carpal height ratio, 4% in the radial inclination, and 9% in the volar tilt. These low values showed a high reliability of the radiographic measurements.

Statistical analysis

All data are represented as mean ± standard deviation. Statistical comparisons were performed using paired *t*-tests. The level of significance was set at $p < .05$.

RESULTS

Clinical assessments

At a mean follow-up of 69 (range, 36–117) months, 6 of the 8 patients were free from pain, and the remaining patients had mild wrist pain on strenuous activity. No patient had pain at the distal radioulnar joint or at the osteotomy site. The mean postoperative range of extension and flexion of the wrist increased significantly, from 91° ± 16° to 151° ± 21° ($p < .01$). The grip strength of the affected side compared with the unaffected side improved from 43% ± 13% to 104% ± 10% ($p < .01$). Based on the scoring system, the mean clinical score was 19.7 (range, 17–21) of 21.0 maximum points. All patients were classified as excellent. There were no postoperative complications.

Radiographic assessments

Bony union at the site of the osteotomy was achieved within 12 weeks in all patients. Radiographic findings suggested that radial shortening prevented disease progression and enhanced diseased lunate revascularization. At follow-up, no progression of Lichtman stages was found in any patient. There were no degenerative changes in the distal radioulnar joint or the radiocarpal joint in any patients. Lunate revascularization, based on the radiographic findings, was found in all patients. Magnetic resonance imaging scans of all patients showed grade V of the Nakamura's grading system, as defined by generalized, low signal intensity of the lunate on T1-weighted and T2-weighted images, before surgery. At follow-up, in 4 of the 6 patients, the MRI

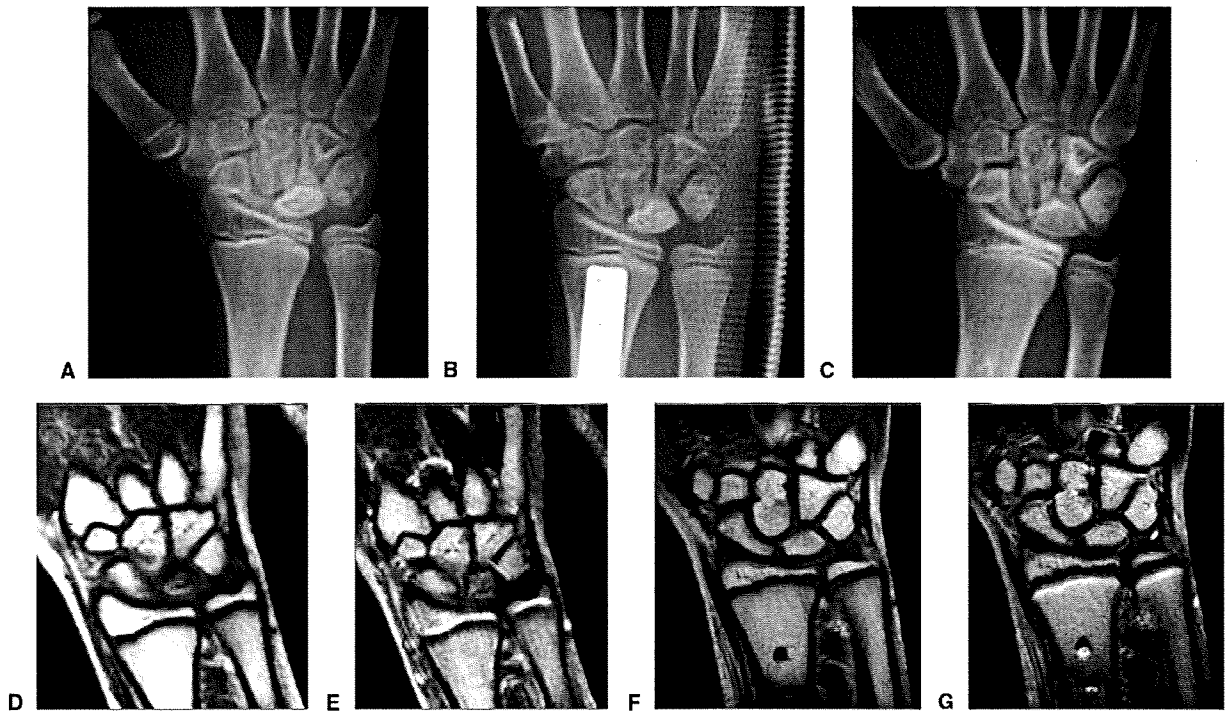

FIGURE 1: A A preoperative AP radiograph of an 11-year-old boy with Stage IIIA Kienböck's disease in the right wrist. **B** The AP radiograph shows ulna-zero variance immediately after radial shortening. **C** The AP radiograph obtained 48 months after radial shortening indicates lunate revascularization with improved appearance of the lunate in density and height. **D, E** Preoperative coronal T1- and T2-weighted MRI images show diffuse decreased signal intensity of the lunate. **F, G** At follow-up, T1- and T2–weighted images demonstrate return of normal signal intensity of the involved lunate.

TABLE 3. Radiographic Parameters

Radiographic Assessment	Before Surgery (Mean ± SD)	Immediately After Surgery (Mean ± SD)	At Follow-Up (Mean ± SD)
Ulnar variance (mm)*	−3.1 ± 1.6	−1.4 ± 1.3	−3.9 ± 2.2
Carpal height ratio	0.47 ± 0.04	0.48 ± 0.04	0.48 ± 0.03
Radial inclination (degrees)	23.8 ± 3.9	23.6 ± 3.9	21.5 ± 4.9
Volar tilt (degrees)	10.0 ± 3.1	8.8 ± 2.6	9.9 ± 3.9

*Denotes statistical significance between "Immediately after Surgery" data and "At Follow-up" data ($p < .05$). Minus numbers refer to negative ulnar variance and positive numbers refer to positive ulnar variance.

scans demonstrated a return of normal marrow signal intensity of the lunate, indicating grade I (Fig. 1). Grade II, including localized regions of slightly decreased signal intensity, was found in the remaining 2 patients.

Postoperative alterations in radiographic parameters showed a tendency toward radial overgrowth after radial shortening for teenagers with Kienböck's disease. Table 3 summarizes the alterations in radiographic parameters. The mean postoperative ulnar variance increased significantly from 1.4 ± 1.3 mm (range, 0–4 mm) of negative ulnar variance to 3.9 ± 2.2 mm (range, 1–8 mm) of negative ulnar variance ($p < .03$). Based on the criteria for overgrowth, 4 of the 8 patients had radial overgrowth on the affected side of the radius (Fig. 2, Table 4). All 4 of these patients were less than 13 years old at the time of surgery. On the other hand, the other parameters showed no notable changes after surgery.

Effect of postoperative radial overgrowth on clinical outcomes

The occurrence of postoperative radial overgrowth did not considerably affect the clinical scores. The mean score was 20.5 ± 0.9 in the patients with radial overgrowth and 19.0 ± 1.6 in those without radial overgrowth.

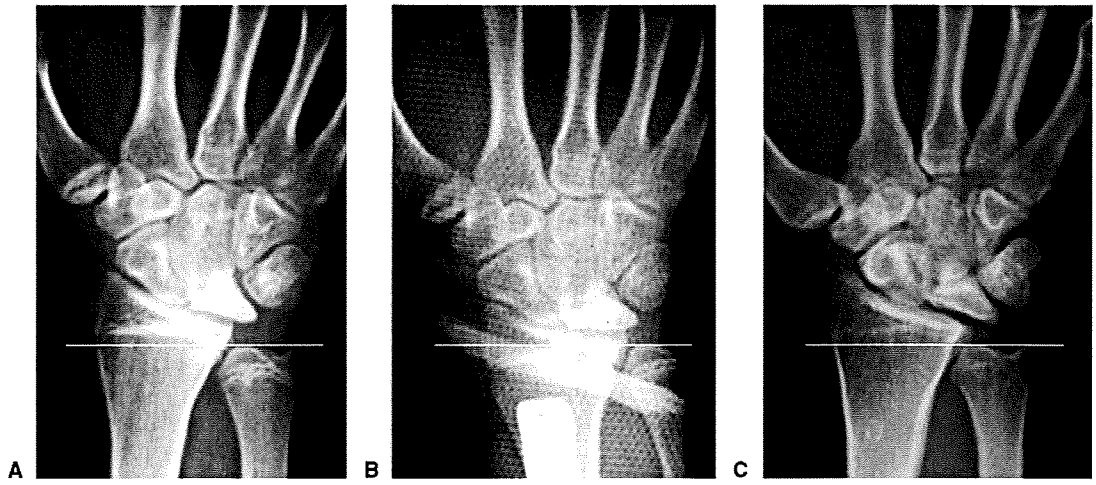

FIGURE 2: A A preoperative AP radiograph of a 13-year-old boy shows Stage IIIB Kienböck's disease in the right wrist. **B** The AP radiograph immediately after radial shortening reveals 1-mm ulna-negative variance. **C** Radial overgrowth at the affected side is found in the AP radiograph at 65 months after radial shortening. The transverse line is set on the tip of ulnar head in **A–C**.

TABLE 4. Changes in Ulnar Variance

Case	Preoperative Lichtman Stage	Age (y)	Follow-Up Period (mo)	Ulnar Negative Variance (mm) Immediately After Surgery	Ulnar Negative Variance (mm) At Follow-Up
1*	II	12	40	3	6
2	II	18	90	1	2
3*	IIIA	11	48	0	4
4*	IIIA	13	48	4	8
5	IIIB	12	113	0	2
6*	IIIB	13	65	1	5
7	IIIB	17	38	1	3
8	IIIB	18	117	0	2

*Denotes overgrowth at follow-up.

DISCUSSION

The first aim of this study was to determine the effect of radial shortening on radial growth in skeletally immature patients with Kienböck's disease. At a mean follow-up of 69 months, in standard radiographs, we recognized that 4 of the 8 patients (50%) had radial overgrowth in the affected side. There were no other findings indicating radial deformities after this surgery. To our knowledge, only 1 case report has demonstrated 8-mm overgrowth at 80 months after radial shortening for Kienböck's disease in a skeletally immature patient.[17]

Carsi et al.[24] showed that 67% of 119 pediatric patients with nonphyseal forearm fracture treated conservatively had radius overgrowth at 5 years after injury. In their study, only fractures in the proximal and middle thirds of the radius were associated with overgrowth; distal third fractures were associated with growth arrest. Our data obtained from the osteotomy cases disagree with these results. One of the reasons for this discrepancy is considered to be the stimulation of growth by surgical procedures. Bone overgrowth is thought to be caused by increased vascularity. Doria et al.[25] showed postoperative hypervascularity after femoral osteotomy in rabbits. This report did not deal with postoperative radius hypervascularity. However, this result may indicate that radial shortening induces hypervascularity of the distal radius. Therefore, we assume that the effects of the radial shortening are considered not only for mechanical decompression but also for increases in distal radius and lunate vascularity. Therefore, stimulation of growth by radial shortening is more likely the cause. Another reason seems to be the existence of microinjuries to the growth plate of the distal radius in distal third fractures. In performing radial shortening, the distal growth plate can be protected from injuries. This could arrest the growth of the radius, even though the radius responds to stimulus caused by fracture.

In this study, radial overgrowth was observed in 4 of 5 patients who were less than 13 years old. A previous case report stated that overgrowth after radial shortening occurred in a 15-year-old boy.[17] Based on the radiographic distance between the distal radius and ulnar growth plates, Pritchett[26] suggested that the skeletal maturation of the forearm bones was at age 13 in girls

and 15 in boys. On the other hand, Carsi et al.[24] concluded that overgrowth after forearm fractures was not influenced by age. Although this contradicts the results mentioned earlier, the probability of radial overgrowth should be considered in doing radial shortening for Kienböck's disease in skeletally immature patients.

Another objective was to clarify the relationships between the postoperative growth changes and the clinical outcomes after radial shortening. In our study, the existence of radial overgrowth did not greatly affect the postoperative clinical outcomes. All skeletally immature patients with postoperative radial overgrowth achieved excellent clinical results. Ulnar negative variance associated with postoperative radial overgrowth seems to cause compressive force to the lunate. This biomechanical effect may lead to the progression of Kienböck's disease. However, the MRI findings obtained in this study indicate that radial shortening produces lunate revascularization and healing in skeletally immature patients with this disease. Consequently, the excessive force produced by radial overgrowth might not advance the stage of Kienböck's disease in skeletally immature patients. Radial shortening provides a positive clinical outcome for skeletally immature patients with Kienböck's disease, despite postoperative radial overgrowth. Therefore, this surgery is considered effective for Kienböck's disease in children. Regarding the surgical technique, we recommend performing a 1- or 2-mm over-shortening for skeletally immature patients, especially those who are less than 13 years old.

This study has considerable limitations. First, the analysis was based on data from a relatively small number of patients. Therefore, the statistical power might not be enough to clearly derive conclusions from this analysis. Second, we had no control group of healthy patients of the same age who did not have surgery. However, we consider that there may be no difference in the laterality of ulnar variance in skeletally immature patients. Therefore, regarding overgrowth, a difference in length of more than 2 mm was considered a discrepancy. Third, at a mean of 69 months after surgery, the radial overgrowth would not produce any radiographic changes, such as osteoarthritis of the distal radioulnar joint and related symptoms. This might not influence the clinical results the same way in the future. A longer follow-up in a large cohort population is needed to overcome these limitations.

REFERENCES

1. Allan CH, Joshi A, Lichtman DM. Kienböck's disease: diagnosis and treatment. J Am Acad Orthop Surg 2001;9:128–136.
2. Eaton RG. Excision and fascial interposition arthroplasty in the treatment of Kienböck's disease. Hand Clin 1993;9:513–516.
3. Kato H, Usui M, Minami A. Long-term results of Kienböck's disease treated by excisional arthroplasty with a silicone implant or coiled palmaris longus tendon. J Hand Surg 1986;11A:645–653.
4. Almquist EE, Burns JF Jr. Radial shortening for the treatment of Kienböck's disease: a 5- to 10-year follow-up. J Hand Surg 1982;7:348–352.
5. Iwasaki N, Minami A, Oizumi N, Suenaga N, Kato H, Minami M. Radial osteotomy for late stage Kienböck's disease: wedge osteotomy versus radial shortening. J Bone Joint Surg 2002;84B:673–677.
6. Iwasaki N, Minami A, Ishikawa J, Kato H, Minami M. Radial osteotomies for teenage patients with Kienböck disease. Clin Orthop 2005;439:116–122.
7. Rock MG, Roth JH, Martin L. Radial shortening osteotomy for treatment of Kienböck's disease. J Hand Surg 1991;16A:454–460.
8. Weiss AP, Weiland AJ, Moore JR, Wilgis EF. Radial shortening for Kienböck disease. J Bone Joint Surg 1991;73A:384–391.
9. Pisano SM, Peimer CA, Wheeler DR, Sherwin F. Scaphocapitate intercarpal arthrodesis. J Hand Surg 1991;16A:328–333.
10. Sennwald GR, Ufenast H. Scaphocapitate arthrodesis for the treatment of Kienböck's disease. J Hand Surg 1995;20A:506–510.
11. Watson HK, Monacelli DM, Milford RS, Ashmead D, IV. Treatment of Kienböck's disease with scaphotrapezio-trapezoid arthrodesis. J Hand Surg 1996;21A:9–15.
12. Hori Y, Tamai S, Okuda H, Sakamoto H, Takita T, Masuhara K. Blood vessel transplantation to bone. J Hand Surg 1979;4:23–33.
13. Hermans S, Degreef I, De Smet L. Vascularised bone graft for Kienböck disease: preliminary results. Scand J Plast Reconstr Surg Hand Surg 2007;41:77–81.
14. Lu LJ, Gong X, Wang KL. Vascularized capitate transposition for advanced Kienböck disease: application of 40 cases and their anatomy. Ann Plast Surg 2006;57:637–641.
15. Hulten O. Anatomical variation of carpal bone. Acta Radiol 1928; 9:155–168.
16. Bonzar M, Firrell JC, Hainer M, Mah ET, McCabe SJ. Kienböck disease and negative ulnar variance. J Bone Joint Surg 1998;80A:1154–1157.
17. Herdem M, Ozkan C, Bayram H. Overgrowth after radial shortening for Kienböck's disease in a teenager: case report. J Hand Surg 2006;31A:1322–1325.
18. Alexander AH, Lichtman DM. Kienböck's disease. In: Lichtman DM, ed. The wrist and its disorders. Philadelphia: WB Saunders, 1998:329–343.
19. Nakamura R, Watanabe K, Tsunoda K, Miura T. Radial osteotomy for Kienböck's disease evaluated by magnetic resonance imaging: 24 cases followed for 1–3 years. Acta Orthop Scand 1993;64:207–211.
20. Gelberman RH, Salamon PB, Jurist JM, Posch JL. Ulnar variance in Kienböck's disease. J Bone Joint Surg 1975;57A:674–676.
21. Chan KP, Huang P. Anatomic variations in radial and ulnar lengths in the wrists of Chinese. Clin Orthop Relat Res 1971;80:17–20.
22. Youm Y, McMurtry RY, Flatt AE, Gillespie TE. Kinematics of the wrist. I. An experimental study of radial-ulnar deviation and flexion-extension. J Bone Joint Surg 1978;60A:423–431.
23. Gartland JJ Jr, Werley CW. Evaluation of healed Colles' fractures. J. Bone Joint Surg 1951;33A:895–907.
24. Carsi B, Abril JC, Epeldegui T. Longitudinal growth after nonphyseal forearm fractures. J Pediatr Orthop 2003;23:203–207.
25. Doria AS, Cunha FG, Modena M, Rodrigues CJ, Garcez AT, Godoy Junior R, et al. Effect of intertrochanteric osteotomy on the proximal femur of rabbits: assessment with power Doppler sonography and scintigraphy. Clinics 2007;62:741–748.
26. Pritchett JW. Growth and development of the distal radius and ulna. J Pediatr Orthop 1996;16:575–577.